ACS Energy LETTERS

http://pubs.acs.org/journal/aelccp

Ultra-stable, Solution-Processable $CsPbBr_3$-SiO_2 Nanospheres for Highly Efficient Color Conversion in Micro Light-Emitting Diodes

Mengda He,[▽] Qinggang Zhang,[▽] Francesco Carulli, Andrea Erroi, Weiyu Wei, Long Kong, Changwei Yuan, Qun Wan, Mingming Liu, Xinrong Liao, Wenji Zhan, Lei Han, Xiaojun Guo, Sergio Brovelli,* and Liang Li*

Cite This: *ACS Energy Lett.* 2023, 8, 151−158

Read Online

ACCESS | Metrics & More | Article Recommendations | Supporting Information

ABSTRACT: **Micro light-emitting diodes (μ-LEDs) coupled to color conversion phosphors are among the most promising technologies for future display and artificial light sources. However, current emitters suffer from excessively large particle sizes, preventing micron-scale processability, and/or low stability that hampers the device lifetime. Here, we demonstrate down-conversion μ-LED phosphors based on $CsPbBr_3$ perovskite nanocrystals directly grown inside perfectly sealed mesoporous silica nanospheres (NSs). Key for this advancement is a high-throughput calcination procedure in the presence of K_2CO_3 as selective pore sealing agent, which simultaneously produces the $CsPbBr_3$ nanocrystals, boosts their emission efficiency to >87%, and perfectly isolates them from the outer environment without causing inter-particle cross-linking or aggregation. This results in size-homogeneous, finely solution-dispersible, ultra-stable, and highly emissive $CsPbBr_3$-SiO_2 NSs that fit the technological requirements of photolithographic inks for highly uniform μ-LED color conversion patterns with pixels smaller than 20 μm.**

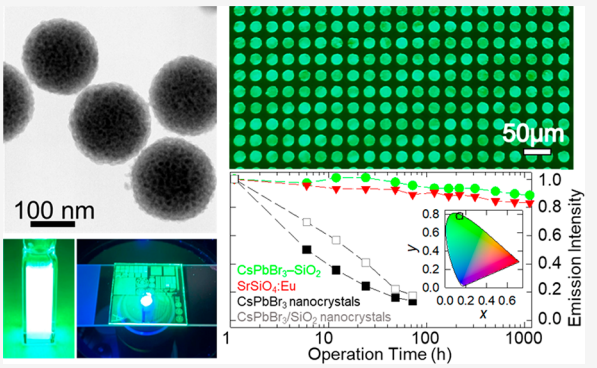

Micro light-emitting diodes (μ-LEDs) are considered the cornerstone devices for future advanced display technology, especially for personalized or wearable devices, such as smart watches and virtual/augmented reality and for ultra-high-definition televisions.[1−3] The most common strategy to achieve full-color μ-LED displays is to combine red, green, and blue (RGB) μ-LEDs, which, however, suffers from difficult mass transfer of RGB chips, the low efficiency of green μ-LED, and driving voltage mismatch between the different pixels.[4−6] Comparatively, applying color conversion layers to UV/blue μ-LEDs requires substantially simpler driving circuitry and avoids cumbersome assembly cycles necessary for the simultaneous transfer of RBG μ-LED arrays.[4,6,7] However, the miniaturization of the LED chip size to below 20 μm requires the formulation of down-conversion phosphors into sufficiently fine inks for incorporation onto tiny chips, as well as high stability for long operation lifetime.[1,6] Currently, color conversion is mainly performed using traditional phosphor micro-powders (typically 1−20 μm), which have poor solution processability and cannot be accurately coupled to blue μ-LEDs chips, making the achievement of high pixel accuracy challenging.[8] Furthermore, conventional phosphors feature a low absorption cross-section and thus cannot efficiently absorb the blue light from chips to guarantee sufficient luminescence intensity necessary for high-resolution displays.[8,9]

The emergence of nanocrystal quantum dots (NCs) is expected to provide a powerful full-color display solution for μ-LED displays owing to their small size (1−10 nm), large light absorption coefficient, high emission color purity, tunability, and high luminescence quantum yield.[10−12] In the past few

Received: September 12, 2022
Accepted: November 8, 2022
Published: November 22, 2022

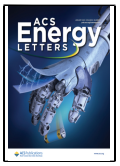

Downloaded via UNIV DEGLI STUDI MILANO-BICOCCA on April 14, 2024 at 19:29:07 (UTC).
See https://pubs.acs.org/sharingguidelines for options on how to legitimately share published articles.

© 2022 The Authors. Published by American Chemical Society

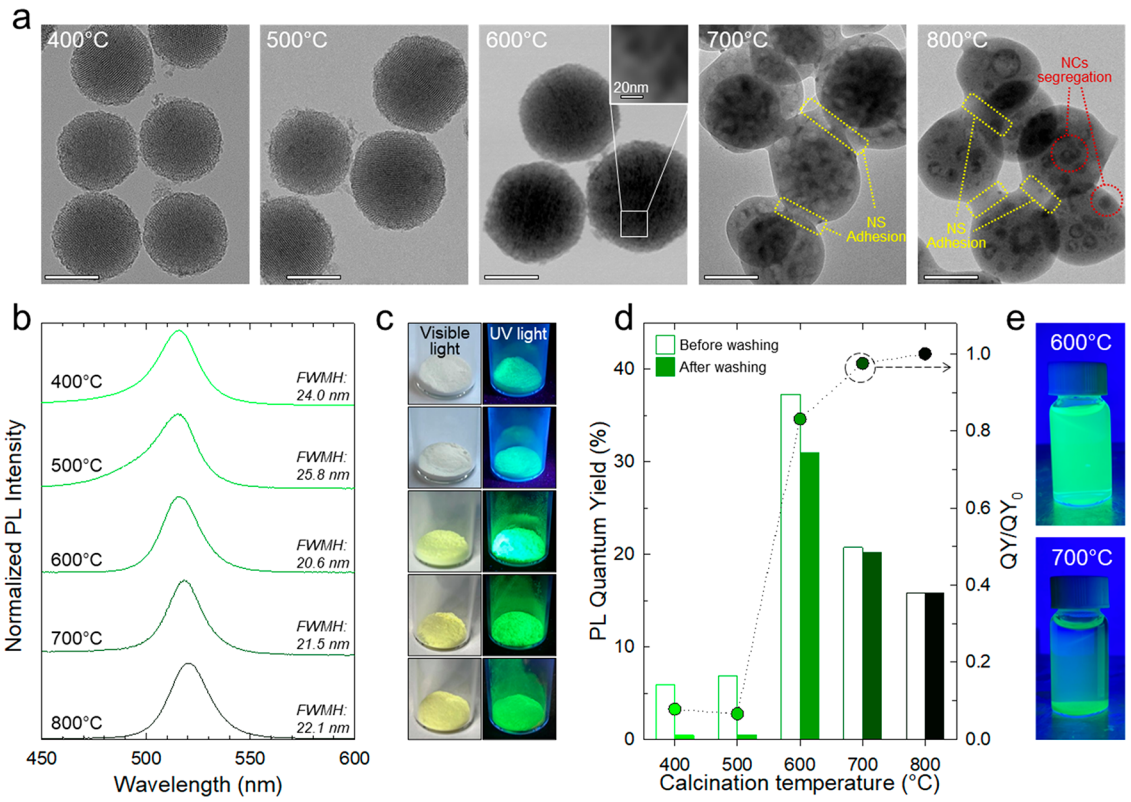

Figure 1. (a) TEM images of $CsPbBr_3$-SiO_2 NSs at different calcination temperatures, namely 400 °C, 500 °C, 600 °C, 700 °C, and 800 °C. Scale bars at the bottom left of the images are 100 nm each. (b) PL spectra of $CsPbBr_3$-SiO_2 NSs at increasing calcination temperature (excitation at 365 nm). (c) Picture of $CsPbBr_3$-SiO_2 NSs powders at increasing calcination temperature under ambient light (left) and UV light (right). (d) PL quantum yield before and after washing with ultra-pure water of $CsPbBr_3$-SiO_2 NSs at different calcination temperatures. (e) Photograph under UV light of $CsPbBr_3$-SiO_2 NSs annealed at 600 °C (top) or 700 °C (bottom) in water, showing the homogeneous dispersion of the first sample and the precipitated particles for the latter.

decades, many colloidal NC systems have been studied for display applications, especially CdSe,[13−15] InP,[16,17] and lead halide perovskite NCs.[18−20] Several strategies have also been proposed to realize NC-based μ-LED displays.[1,6,21−24] However, almost all studies reported short device life or avoided addressing the general aspect of operational stability because it requires complicated device encapsulation or NC protection strategies (e.g., using inert shells of polymer, SiO_2, Al_2O_3, etc.) to withstand the harsh "on-chip" conditions.[25−29] In fact, conventional coating methods based on room-temperature colloidal processes yield insufficiently compact coating layers to match the high stability requirements of μ-LEDs applications.[30,31]

Recently, we demonstrated stable $CsPbBr_3$ QDs-SiO_2 ceramic particles produced via solid-state NCs growth using mesoporous silica templates, which combine the excellent optical properties of perovskite NCs[31−36] in one of the most stable nanomaterials available to date. Other research groups also demonstrated that high-quality $CsPbX_3$ NCs can be synthesized in host matrixes, such as metal−organic frameworks (MOFs), glasses, and metal oxides.[37−41] Although successful in protecting the QDs from the environment, all these approaches, including ours, produce overly large particles (>2 μm) or even bulk glasses, which makes them unsuitable for uniform embedding into tiny μ-LED chips.[1,6] Therefore, all currently available color conversion materials, including conventional ceramic phosphors (too large size), conventional or perovskite NCs (unstable), and perovskite composites and glasses (too large size), cannot simultaneously fulfill the optical, stability, and particle size requirements for successful applications in μ-LEDs.

Here, we propose a high-throughput strategy to synthesize solution-dispersible, size-uniform, highly luminescent, and ultra-stable $CsPbX_3$-SiO_2 nanospheres (NSs, diameter = 200 nm) by selective sintering in mesoporous silica nanoparticles (MSNs) in the presence of K_2CO_3, which both seals the inner pores of the MSNs and passivates detrimental surface defects of the inner $CsPbBr_3$ NCs. As a result, our $CsPbBr_3$-SiO_2 NSs show photoluminescence quantum yield (PLQY) as high as 87 ± 5%, narrow emission spectrum (fwhm ≈ 22 nm), and exceptional chemical and photo-stability comparable to those of commercial ceramic Sr_2SiO_4:Eu^{2+} green phosphor. Finally, we processed our NSs in photolithographic inks that demonstrate substantially better film-forming ability compared to commercial Sr_2SiO_4:Eu^{2+} or other micron-scale $CsPbBr_3$-based phosphors and enable us to produce highly uniform and luminescent 10−50 μm sized μ-LEDs via solution patterning.

Synthesis and Properties of $CsPbBr_3$ NCs inside MSNs. The particle size and dispersion of fluorescent materials are key parameters for their solution processability. To this end, we synthesized a series of uniform MSNs following a modified protocol,[42] which were then employed as nano-templates for the confined growth of $CsPbBr_3$ NCs. The MSNs exhibited uniform size of 200 ± 26 nm (Figure S1) with long-range ordered pore structures and large specific surface area (Table S1). To synthesize the $CsPbBr_3$-SiO_2 NSs, the MSNs template was first soaked in the precursor salts (CsBr and $PbBr_2$) solution and then dried at 80 °C. The resultant mixture

https://doi.org/10.1021/acsenergylett.2c02062
ACS Energy Lett. 2023, 8, 151−158

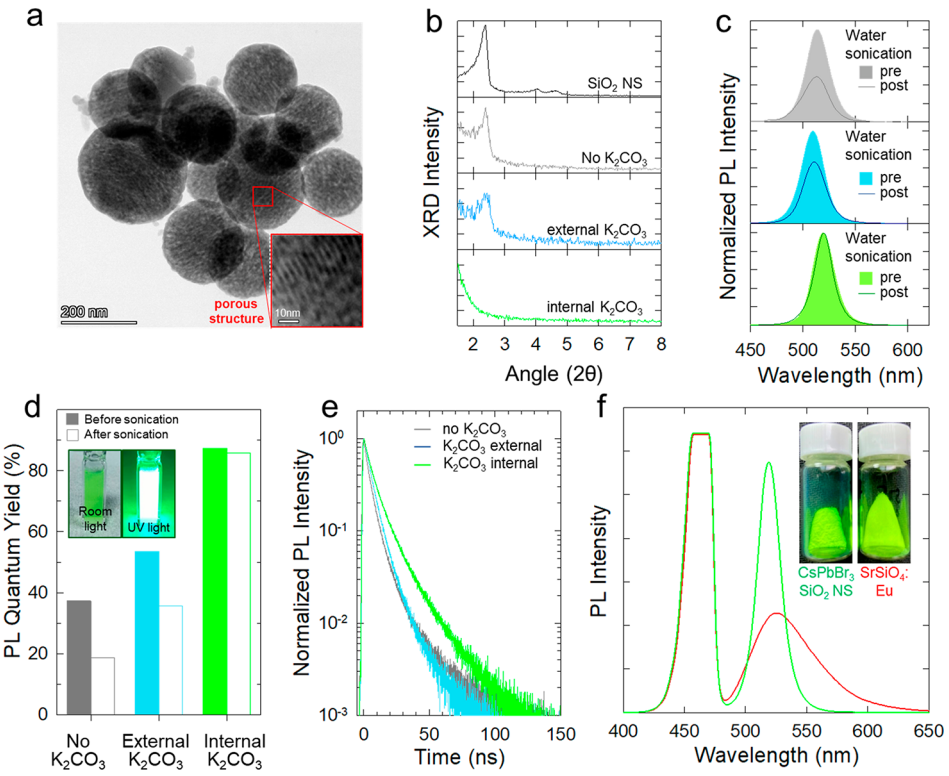

Figure 2. (a) TEM image of $CsPbBr_3$-SiO_2 NSs sintered at 600 °C with the "external" addition of K_2CO_3 (K:$CsPbBr_3$ 1:1 mol/mol). (b) Comparison between small-angle XRD patterns of $CsPbBr_3$-SiO_2 NSs with different K_2CO_3 treatment: without K_2CO_3 (gray curve), with external (blue curve) or internal (green curve) addition of K_2CO_3. The XRD pattern for template SiO_2 MSN is reported as a black curve. The same color code applies to panels b–e. (c) PL spectra and (d) PLQY of the same NS samples as in panel b before and after sonication in water for 20 h. Inset of panel d: photograph of internally sintered $CsPbBr_3$-SiO_2 NSs dispersed in water under room light and under 365 nm UV radiation. (e) PL decay traces of the same samples as in panels b and c. (f) PL spectrum of internally sintered $CsPbBr_3$-SiO_2 NSs compared to the Sr_2SiO_4:Eu^{2+} green phosphor under identical 455 nm excitation and collection geometry. Inset: photograph of the two phosphor powders under room light.

was placed into a furnace and heated to 400–800 °C. The cooled samples were washed with ultra-pure water and dried to obtain the target product (Figure 1a).

The X-ray diffraction (XRD) patterns (Figure S2) confirmed the successful formation of cubic $CsPbBr_3$ NCs inside the MSNs. Transmission electron microscopy (TEM) images of $CsPbBr_3$-SiO_2 powders at increasing calcination temperature from 400 °C to 800 °C are reported in Figure 1a, showing distinct crystalline $CsPbBr_3$ NCs inside the NSs sintered up to 600 °C and non-homogeneous agglomerates of $CsPbBr_3$ NCs for higher temperatures. The corresponding PL spectra are reported in Figure 1b showing, in all cases, the typical emission profile of $CsPbBr_3$ NCs. The PL spectra gradually red shift, indicating progressive particle growth with increasing temperature and a non-monotonic trend of the spectral line width, with the NSs calcinated at 600 °C featuring the narrowest profile. This suggests poor formation of the perovskite NCs at the lowest calcination temperatures (400–500 °C) causing the noticeable asymmetry of the respective PL spectra and the low PL quantum yield (PLQY < 10%, Figure 1c). On the other hand, the NSs prepared at 600 °C show a narrow and symmetrical PL spectrum and the highest emission efficiency in the series (PLQY = 37%). Further increasing the calcination temperature to 700–800 °C results in the gradual broadening of the PL profiles and the drop of the PLQY to 20% and 16%, respectively. This behavior is consistent with high temperatures favoring the segregation of larger $CsPbBr_3$ domain NCs inside the MSN and the formation of the non-emissive Cs_4PbBr_6 phase, as highlighted by the optical absorption spectra in Figure S3.

Also fundamentally, the calcination temperature plays a decisive role in the processability in solution and in the conservation of the optical properties following the dispersion of NSs in water. Specifically, as shown in Figure 1a,d, NSs synthesized at lower temperatures (400, 500 °C) kept the single-particle morphology, but their porous structure did not collapse, resulting in poor water resistance due to dissolution of the embedded $CsPbBr_3$ NCs. On the other hand, the highest sintering temperatures (700, 800 °C) sealed all pores and buried the $CsPbBr_3$ NCs inside the particle, resulting in retained PL intensity after washing in water. However, such high sintering temperatures also caused the aggregation of MSNs powders into large, cross-linked particles (Figure 1a), which could not be dispersed in solution even after intense sonication (Figure 1e). In contrast, the NSs calcinated at 600 °C maintained their original single-particle morphology and could be easily dispersed into water by sonication, forming a stable clean suspension. This indicated at 600 °C the limit of low calcination temperature to synthesize $CsPbBr_3$-SiO_2 NSs with high PLQY and good dispersibility. Nonetheless, the still incomplete collapse of their porous structure led to ∼20% PL quenching upon dissolution in water (Figure 1d).

In order to achieve both high stability and solution dispersibility, it was therefore necessary to develop a finer pore-sealing strategy than high-temperature annealing that also prevented particles from fusing together. With this in mind,

https://doi.org/10.1021/acsenergylett.2c02062
ACS Energy Lett. 2023, 8, 151–158

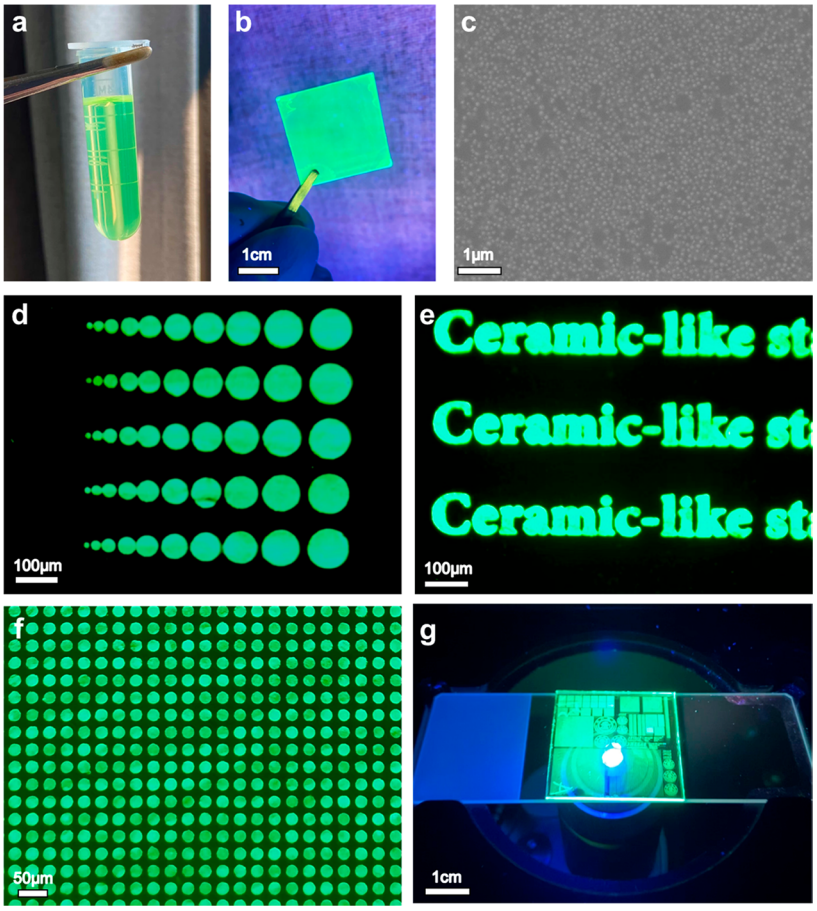

Figure 3. (a) Optical image of photolithographic ink fabricated using $CsPbBr_3$-SiO_2 NSs under room light. (b) Optical image of the thin film fabricated using the $CsPbBr_3$-SiO_2 NSs ink under UV lamp excitation (365 nm). (c) SEM image of the thin film fabricated by spin-coating on a glass substrate. (d) Fluorescent images of $CsPbBr_3$-SiO_2 NSs-based pixels with diameters varying from 10 to 100 μm. (e) Fluorescent images of $CsPbBr_3$-SiO_2 English words. (f) Fluorescent images of 20 μm pixel array based on $CsPbBr_3$-SiO_2 NSs. (g) Optical image of $CsPbBr_3$-SiO_2 patterns on a 1-in. glass substrate under 365 nm UV lamp excitation.

and inspired by sintering methods used for films or mesoporous particles that employ low-melting-point salts as the flux agent to initiate surface melting or bonding through the solid−liquid interface,[43−46] we overcame this limitation by adding potassium carbonate (K_2CO_3) into the mixture of precursor solution and MSNs before drying. This selectively promoted the complete collapse of the internal pores of the MSNs template already at 600 °C annealing temperature, thus preventing concurrent particle agglomeration. The TEM images, high-angle annular dark-field scanning transmission electron microscopy (HAADF-STEM), and elemental mapping of such "internally" K_2CO_3-sintered $CsPbBr_3$-SiO_2 NSs (to be distinguished from the "externally" K_2CO_3-sintered NSs discussed in the following) are reported in Figure S4, showing particles with completely collapsed internal pores containing evenly distributed crystalline $CsPbBr_3$ NCs with size $d = 8.6 \pm 1.3$ nm (Figure S5). When the amount of K_2CO_3 was further increased to 2:1 and 4:1 mol/mol (K:$CsPbBr_3$), particle cross-linking and fusing occurred (Figure S6).

To highlight the importance of adding K_2CO_3 to the mixture of precursor solution and MSNs before drying, we further performed a control experiment where K_2CO_3 was mixed with dried pre-synthesized $CsPbBr_3$-SiO_2 NSs through a physical grinding method (the obtained sample is hereafter referred to as "externally" K_2CO_3-sintered NSs). As sketched in Figure S7, in this case, solid K_2CO_3 crystals or micro-powders could not enter the nanometric pores, resulting in K_2CO_3 being only on the outer surface of the MSNs particles. After calcination at 600 °C of such externally sintered NSs, agglomeration occurred (Figure 2a), but the internal pores still did not collapse, same as in the original NSs without K_2CO_3, as further confirmed by small-angle XRD patterns (Figure 2b).

More importantly, water resistance experiments (sonicating in water for 20 h) on internally K_2CO_3-sintered NSs showed essentially no drop of the PL intensity, thus confirming the outstanding protective effect on the inner $CsPbBr_3$ NCs by the fully collapsed pores (Figure 2c,d). On the other hand, the external addition of K_2CO_3 did not prevent water from damaging the $CsPbBr_3$ NCs because of the incomplete collapse of the pore structure (inset of Figure 2a). Fundamentally, as shown in Figure 2d, internal K_2CO_3 sintering not only substantially enhanced the resistance toward water of $CsPbBr_3$-SiO_2 NSs but also largely boosted their PLQY. Compared with original $CsPbBr_3$-SiO_2 NSs (PLQY = 37%), the sample produced via external K_2CO_3 sintering showed PLQY = 51%, and internally K_2CO_3-sintered NSs featured a much higher PLQY = 87%. One possible cause of this further important benefit of internal K_2CO_3 sintering is suggested by the XRD patterns reported in Figure S8, showing that the introduction of K_2CO_3 induced the formation of a Cs_4PbBr_6 phase, which has been previously demonstrated to bind to $CsPbBr_3$ and form a Type I junction that passivates surface

https://doi.org/10.1021/acsenergylett.2c02062
ACS Energy Lett. 2023, 8, 151−158

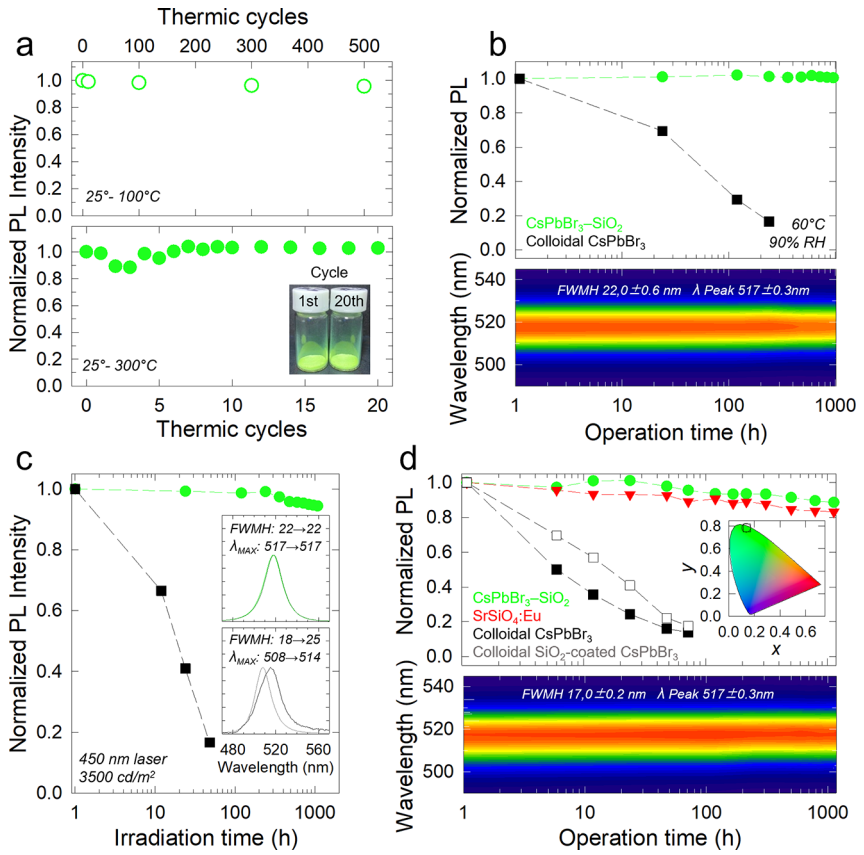

Figure 4. (a) Normalized PL intensity of internally K_2CO_3-sintered $CsPbBr_3$-SiO_2 NSs collected during 500 cycles of 25−100 °C thermal treatment (top) in flowing Ar and during 20 cycles of 25−300 °C annealing (bottom) in a muffle furnace in air atmosphere. (b) Top panel: Normalized PL intensity of PMMA films containing $CsPbBr_3$-SiO_2 (green dots) and colloidal $CsPbBr_3$ NCs (black squares) aged at 60 °C and 90% relative humidity. Bottom panel: contour plot of $CsPbBr_3$-SiO_2 PL spectra collected during the same aging experiment. The same color code applied to all plots in the figure. (c) PL stability of PMMA film containing K_2CO_3-sintered $CsPbBr_3$-SiO_2 and colloidal $CsPbBr_3$ NCs under continuous LED irradiation (405 nm, 3500 cd/m^2). In the inset, the initial (0 h, light lines) and final (1080 h, dark lines) normalized PL spectra of tested films are reported together with PL emission features. (d) Top: PL stability of $CsPbBr_3$-SiO_2 (green circles), commercial Sr_2SiO_4:Eu^{2+} phosphor (red triangles), $CsPbBr_3$ colloidal NCs (black filled squares), and SiO_2-coated $CsPbBr_3$ colloidal NCs (empty gray squares) sealed with UV glue on a blue LED chip (20 mA, 2.7 V, 1.3 mm × 1.3 mm) in ambient air. Bottom panel: contour plot of $CsPbBr_3$-SiO_2 PL spectra collected at increasing operation time. In the inset is reported the CIE diagram of $CsPbBr_3$-SiO_2 NSs before (circle) and after (square) 1080 h of operation time (x = 0.137, y = 0.784 and x = 0.142, y = 0.785, respectively).

defects and dramatically improves the PLQY.[47,48] This scenario is corroborated by the time decay PL curves reported in Figure 2e, showing that original $CsPbBr_3$-SiO_2 NSs featured a slight multi-exponential decay dynamics with an effective lifetime (extracted as the time after which the PL intensity has dropped by a factor e) of 4.7 ns and a longer-lived tail, commonly ascribed to regenerated band edge excitons by back-transfer from shallow traps. The addition of K_2CO_3 turned the decay kinetics more single exponential and extended the lifetime to 6.2 ns for the externally K_2CO_3-sintered particles, up to 8.1 ns for the internally sintered NSs.

As a result of the positive effect of internal K_2CO_3 sintering, $CsPbBr_3$-SiO_2 NSs (Figure 2f) showed comparable green fluorescence to the commercial green-emitting Sr_2SiO_4:Eu^{2+} phosphor (Intematix Co.), even under room light illumination. Notably, due to their much higher color purity (fwhm = 22.7 nm vs 62.5 nm), the peak intensity of $CsPbBr_3$-SiO_2 NSs was nearly twice as high as that of Sr_2SiO_4:Eu^{2+} phosphors. Furthermore, the internally K_2CO_3-sintered $CsPbBr_3$-SiO_2 dispersed in water formed uniform, transparent, and highly emissive solutions with PLQY exceeding 90% owing to lower self-absorption compared to the powder sample.[40] We highlight that the strategy of selective pore collapse assisted by K_2CO_3 can be also applied to orange- or red-emitting $CsPbBr_{1.5}I_{1.5}$ and $CsPbI_3$ NCs (Figure S9), indicating the universality of the proposed strategy. We finally notice that the analogous annealing procedure could be, in principle, performed using $CsCO_3$ and $NaCO_3$ as sintering agents. However, preliminary studies adopting the exact same condition as with K_2CO_3 result in excessive inter-particle agglomeration using $NaCO_3$ and strong formation of non-emitting Cs_4PbBr_6 NCs phase due to the excess cesium when using $CsCO_3$, in either case lowering the emission efficiency (see Figures S10 and S11).

Solution Processability and Photolithographic Patterning. Returning to the goal of creating color conversion layers for μ-LEDs using solution techniques, we evaluated the solution-processing potential of our internally K_2CO_3-sintered NSs and found that they can be uniformly and consistently dispersed in water or ethanol by simple sonication, producing almost no settlement after a full 150 days (Figure S12; hereafter all NSs are intended as internally K_2CO_3-sintered).

In order to test their suitability for high-resolution patterning of color-converting layers, we opted for photo-

https://doi.org/10.1021/acsenergylett.2c02062
ACS Energy Lett. 2023, 8, 151−158

lithography, as it provides high patterning quality, productivity, and reproducibility.[22,49,50] We then fabricated a photolithographic ink (Figure 3a) by mixing NSs with a photoresist (SU-8 2002) and used it to produce highly uniform films by spin-coating on a glass substrate (Figure 3b). The notable film-forming ability of the ink was further confirmed by scanning electron microscopy (SEM), showing a uniform dispersion of NSs inside the photoresist (Figure 3c and Figure S13), which is vital for producing high-quality/resolution color-converting layers. Finally, by applying photomasks, we realized the micro-patterned color-converting layer reported in Figure 3d−g. Specifically, Figure 3d shows fluorescent images of pixels with diameter varying from 10 to 100 μm. Pixel arrays of 20 μm and 50 μm were successfully achieved, as shown in Figure 3f and Figure S14a. Examples of English words and the SJTU logo are presented in Figure 3e and Figure S14b. All of these images exhibit strong green luminescence with high color contrast, indicating that our composites can achieve high-resolution ($\leq$20 μm) pixel patterning that satisfies the requirements for μ-LEDs via photolithography. By contrast, Sr_2SiO_4:Eu^{2+} and $CsPbBr_3$ grown into common mesoporous silica (MCM) particles showed substantially worse film-forming ability and consequently lower-quality patterns (Figure S15).

Stability of $CsPbBr_3$-SiO_2 NS. The maintenance of high luminescence performance is crucial for the implementation of chromophores as color-converting layers in μ-LEDs. For this reason, we studied the stability of our NSs in different environmental and operational conditions (in this section, all $CsPbBr_3$-SiO_2 NSs are intended as internally K_2CO_3-sintered). First, we monitored the emission stability of NSs when stored in ambient conditions or solubilized in acid and basic aqueous solutions (i.e., 1 M HCl or 0.1 M NaOH), and we found that $CsPbBr_3$-SiO_2 NSs preserve nearly 100% of their initial PL efficiency in all conditions (Figure S16), in agreement with recent reports on encapsulated lead halide perovskite NCs.[31,36−38] The morphology of the $CsPbBr_3$ NCs embedded inside the NSs did not change after as long as 20 min of high-energy electron beam irradiation (1.05 Mx, 0.7 nA, 6500 e $Å^{-2}$ s^{-1}), and the 0.33 nm inter-plane lattice distance corresponding to the lattice fringes of the (111) direction could still be observed. This is surprising, as the same test on conventional colloidal $CsPbBr_3$ NCs revealed morphological changes within just 20 s of irradiation (Figure S17), in agreement with the known fragility of lead halide perovskites under intense electron beams.

One of the most important aspects to consider when evaluating the applicability of this technology in real devices is the possible leakage of Pb^{2+} from $CsPbBr_3$ during operation or end-of-life. To assess this aspect, we immersed 100 mg powder of our $CsPbBr_3$-SiO_2 NSs in 50 mL ultrapure water and sampled the concentration of aqueous Pb^{2+} periodically by inductively coupled plasma-optical emission spectrometry (ICP-OES). Notably, no traces of Pb^{2+} leakage were detected after as long as 1200 h (Figure S18), indicating that encapsulation into densified silica renders our powder safe and environmentally friendly. Possibly more importantly for their application in real μ-LED devices, we evaluated the thermal stability of $CsPbBr_3$-SiO_2 NSs. For this purpose, we monitored the PL intensity during a series of moderate (up to 100 °C) and high (up to 300 °C) temperature annealing cycles. As reported in Figure 4a, in both cases, the NSs emission is perfectly unaltered. This result is further confirmed by thermogravimetric analysis, showing negligible weight loss up to 660 °C (Figure S19). Next, we took into consideration the practical aspects of the realization of display or lighting devices, such as "chip on board packaging" or "quantum-dot enhanced film", typically involving fluorescent materials mixed with curing resins or polymers to produce color-converting layers, whose stability is crucial for the lifetime of the final products.

For this purpose, we aged a UV-cured poly(methyl methacrylate) (PMMA) film containing $CsPbBr_3$-SiO_2 NSs at 60 °C and 90% relative humidity for 1000 h. As can be seen in Figure 4b, the film retained 100% of its initial PL intensity and showed no measurable spectral modification in terms of both peak wavelength and width (see the contour plots of the PL spectra vs time), indicating a remarkable temperature and moisture resistance. Also crucially, using a blue LED (450 nm, 3500 cd/m^2) as a backlight to simulate the working conditions of a color-converted μ-LEDs revealed that the $CsPbBr_3$-SiO_2 NSs/PMMA film preserved as much as 94% of its initial emission intensity and perfect spectral properties after 1000 h of continuous illumination (Figure 4c). In contrast, a PMMA film containing colloidal $CsPbBr_3$ NCs suffered >80% PL drop and a measurable red-shift of the PL spectrum in less than 100 h. Finally, to assess the potential of $CsPbBr_3$-SiO_2 NSs powders sealed with UV glue (PMMA) as the color conversion layer was directly coated on top of a blue LED chip, we tested their operational stability under 455 nm illumination (20 mA and 2.7 V) at room temperature. Colloidal $CsPbBr_3$ NCs, SiO_2-coated $CsPbBr_3$ NCs, and ceramic Sr_2SiO_4:Eu^{2+} phosphors were used as control samples. Also in this case, $CsPbBr_3$-SiO_2 NSs showed superior stability (1000 h, PL drop < 12%), which even slightly surpassed that of commercial Sr_2SiO_4:Eu^{2+} green phosphor (Figure 4d). In contrast, the PL intensity of colloidal $CsPbBr_3$ NCs and SiO_2-coated $CsPbBr_3$ NCs sharply dropped to 16% and 22% after 48 h, respectively. In addition to this, the $CsPbBr_3$-SiO_2 NSs did not suffer from any modification of their emission spectrum, resulting in identical CIE color coordinates before and after 1000 h of operation (inset of Figure 4d and Figure S20). This remarkable performance further indicates that the NSs with selectively collapsed inner pores are dense and rigid enough to prevent the penetration of oxygen, moisture, as well as detrimental heating effects in practical display applications.

In summary, we synthesized highly luminescent (PLQY > 87%), solution-dispersible, ultra-stable $CsPbBr_3$-SiO_2 NSs with uniform small size (200 nm) by a selective sintering strategy using K_2CO_3 to completely seal the internal pores of SiO_2 MSNs particles without causing particle cross-linking and aggregation. Leveraging these remarkable features, we then used these new phosphors for formulating an unprecedented $CsPbBr_3$ NCs-based photolithographic ink for the fabrication of μ-LED conversion patterns with pixels smaller than 20 μm. For all these reasons, we strongly believe that our results will have a remarkable impact on future progress in μ-LED technologies.

■ ASSOCIATED CONTENT

Supporting Information

The Supporting Information is available free of charge at https://pubs.acs.org/doi/10.1021/acsenergylett.2c02062.

Detailed description of the NSs synthesis and experimental methods, characterization data such as MSN and NC size distribution, XRD and optical absorption vs

https://doi.org/10.1021/acsenergylett.2c02062
ACS Energy Lett. 2023, 8, 151−158

calcination temperature, elemental mapping, NSs calcinated using Na_2CO_3 or Cs_2CO_3, $CsPbI_3$-SiO_2 NSs, SEM of a polymeric film containing $CsPbBr_3$-SiO_2 NSs, and stability in acidic and basic solutions, including Table S1 and Figures S1−S20 (PDF)

AUTHOR INFORMATION

Corresponding Authors

Sergio Brovelli − *Dipartimento di Scienza dei Materiali, Università degli Studi di Milano-Bicocca, 20125 Milan, Italy*; Email: sergio.brovelli@unimib.it

Liang Li − *School of Environmental Science and Engineering, Shanghai Jiao Tong University, Shanghai 200240, China; Macao Institute of Materials Science and Engineering (MIMSE), MUST-SUDA Joint Research Center for Advanced Functional Materials, Zhuhai MUST Science and Technology Research Institute, Macau University of Science and Technology, Taipa 999078 Macao, China*; orcid.org/0000-0003-3898-0641; Email: lli@must.edu.mo

Authors

Mengda He − *School of Environmental Science and Engineering, Shanghai Jiao Tong University, Shanghai 200240, China*

Qinggang Zhang − *School of Environmental Science and Engineering, Shanghai Jiao Tong University, Shanghai 200240, China; Department of Electronic Engineering, School of Electronics Information and Electrical Engineering, Shanghai Jiao Tong University, Shanghai 200240, China*

Francesco Carulli − *Dipartimento di Scienza dei Materiali, Università degli Studi di Milano-Bicocca, 20125 Milan, Italy*; orcid.org/0000-0002-8345-6606

Andrea Erroi − *Dipartimento di Scienza dei Materiali, Università degli Studi di Milano-Bicocca, 20125 Milan, Italy*

Weiyu Wei − *School of Chemistry and Chemical Engineering, Shanghai Jiao Tong University, Shanghai 200240, China*

Long Kong − *School of Environmental Science and Engineering, Shanghai Jiao Tong University, Shanghai 200240, China*

Changwei Yuan − *School of Environmental Science and Engineering, Shanghai Jiao Tong University, Shanghai 200240, China*

Qun Wan − *School of Environmental Science and Engineering, Shanghai Jiao Tong University, Shanghai 200240, China*

Mingming Liu − *School of Environmental Science and Engineering, Shanghai Jiao Tong University, Shanghai 200240, China*

Xinrong Liao − *School of Environmental Science and Engineering, Shanghai Jiao Tong University, Shanghai 200240, China*

Wenji Zhan − *School of Environmental Science and Engineering, Shanghai Jiao Tong University, Shanghai 200240, China*

Lei Han − *Department of Electronic Engineering, School of Electronics Information and Electrical Engineering, Shanghai Jiao Tong University, Shanghai 200240, China*

Xiaojun Guo − *Department of Electronic Engineering, School of Electronics Information and Electrical Engineering, Shanghai Jiao Tong University, Shanghai 200240, China*

Complete contact information is available at: https://pubs.acs.org/10.1021/acsenergylett.2c02062

Author Contributions

▽M.H. and Q.Z. contributed equally.

Notes

The authors declare no competing financial interest.

ACKNOWLEDGMENTS

This work was supported by the “Pioneer” and "Leading Goose" R&D Program of Zhejiang (2022C03187); the National Natural Science Foundation of China (NSFC 22175113, 42007125, 22205136); the China Postdoctoral Science Foundation (2021M702115); Shanghai Post-doctoral Excellence Program (2021239); Joint Funds of the National Natural Science Foundation of China (No.U21A20320). We thank Weilin Zheng and Ruixin Yan from the Department of Materials Science and Engineering of City University of Hong Kong for help with the TEM and ICP-OES measurements. We thank Baijiang Bao from the School of Design of Shanghai Jiao Tong University for help with the design of schematic diagram. We thank Fu Wang and Dan Zhao from the School of Biomedical Engineering of Shanghai Jiao Tong University for help with the Fluorescent microscope measurement. We also thank Chen Zou from the College of Optical Science and Engineering of Zhejiang University for help with the design of photomasks.

REFERENCES

(1) Liu, Z.; et al. Micro-light-emitting diodes with quantum dots in display technology. *Light: Sci. Appl.* **2020**, *9*, 83.

(2) Zhang, K.; et al. Fully-integrated active matrix programmable UV and blue micro-LED display system-on-panel (SoP). *J. Soc. Inf. Dispersion* **2017**, *25* (4), 240−248.

(3) Zhang, X.; et al. Active matrix monolithic LED micro-display using GaN-on-Si epilayers. *IEEE Photon. Technol. Lett.* **2019**, *31* (11), 865−868.

(4) Cho, J.; et al. White light-emitting diodes: history, progress, and future. *Laser Photon. Rev.* **2017**, *11* (2), 1600147.

(5) Huang, J.; et al. Mini-LED, Micro-LED and OLED displays: present status and future perspectives. *Light: Sci. Appl.* **2020**, *9*, 105.

(6) Zhou, X.; et al. Growth, transfer printing and colour conversion techniques towards full-colour micro-LED display. *Prog. Quantum Electron.* **2020**, *71*, 100263.

(7) Zhang, H.; Rogers, J. A. Recent advances in flexible inorganic light emitting diodes: From materials design to integrated optoelectronic platforms. *Adv. Opt. Mater.* **2019**, *7* (2), 1800936.

(8) Lin, C. C.; Liu, R.-S. Advances in Phosphors for Light-emitting Diodes. *J. Phys. Chem. Lett.* **2011**, *2* (11), 1268−1277.

(9) Fang, M.-H.; et al. Evolutionary Generation of Phosphor Materials and Their Progress in Future Applications for Light-Emitting Diodes. *Chem. Rev.* **2022**, *122* (13), 11474−11513.

(10) Bourzac, K. Quantum dots go on display. *Nature* **2013**, *493* (7432), 283−283.

(11) Shirasaki, Y.; et al. Emergence of colloidal quantum-dot light-emitting technologies. *Nat. Photonics* **2013**, *7* (1), 13−23.

(12) Gandini, M.; et al. Efficient, fast and reabsorption-free perovskite nanocrystal-based sensitized plastic scintillators. *Nat. Nanotechnol.* **2020**, *15* (6), 462−468.

(13) Li, Z.; et al. General Method for the Synthesis of Ultrastable Core/Shell Quantum Dots by Aluminum Doping. *J. Am. Chem. Soc.* **2015**, *137* (39), 12430−12433.

(14) Dai, X.; et al. Solution-processed, high-performance light-emitting diodes based on quantum dots. *Nature* **2014**, *515* (7525), 96−99.

(15) Cui, J.; et al. Efficient light-emitting diodes based on oriented perovskite nanoplatelets. *Sci. Adv.* **2021**, *7* (41), No. eabg8458.

(16) Won, Y.-H.; et al. Highly efficient and stable InP/ZnSe/ZnS quantum dot light-emitting diodes. *Nature* **2019**, *575* (7784), 634−638.
(17) Jeong, B. G.; et al. Interface polarization in heterovalent core-shell nanocrystals. *Nat. Mater.* **2022**, *21* (2), 246−252.
(18) Liu, X.-K.; et al. Metal halide perovskites for light-emitting diodes. *Nat. Mater.* **2021**, *20*, 10−21.
(19) Dong, Y.; et al. Bipolar-shell resurfacing for blue LEDs based on strongly confined perovskite quantum dots. *Nat. Nanotechnol.* **2020**, *15* (8), 668−674.
(20) Wang, K.; Dou, L. Colloidal nanocrystals for large-area LEDs. *Nat. Nanotechnol.* **2022**, *17* (6), 562−563.
(21) Yin, Y.; et al. Full-Color Micro-LED Display with $CsPbBr_3$ Perovskite and CdSe Quantum Dots as Color Conversion Layers. *Adv. Mater. Technol.* **2020**, *5* (8), 2000251.
(22) Zou, C.; et al. Photolithographic Patterning of Perovskite Thin Films for Multicolor Display Applications. *Nano Lett.* **2020**, *20* (5), 3710−3717.
(23) Lin, H.-Y.; et al. Optical cross-talk reduction in a quantum-dot-based full-color micro-light-emitting-diode display by a lithographic-fabricated photoresist mold. *Photon. Res.* **2017**, *5* (5), 411−416.
(24) Hwangbo, S.; et al. Wafer-scale monolithic integration of full-colour micro-LED display using MoS_2 transistor. *Nat. Nanotechnol.* **2022**, *17*, 500−506.
(25) Chen, H.; et al. Recent Advances on Quantum-Dot-Enhanced Liquid-Crystal Displays. *IEEE J. Sel. Top. Quantum Electron.* **2017**, *23* (5), 1900611.
(26) Coe-Sullivan, S.; et al. Quantum Dots for LED Down-conversion in Display Applications. *ECS J. Solid State Sci. Technol.* **2013**, *2* (2), R3026−R3030.
(27) Kang, C.; et al. Quantum-Rod On-Chip LEDs for Display Backlights with Efficacy of 149 lm W^{-1}: A Step toward 200 lm W^{-1}. *Adv. Mater.* **2021**, *33*, 2104685.
(28) Zhang, D.; et al. Large-scale planar and spherical light-emitting diodes based on arrays of perovskite quantum wires. *Nat. Photonics* **2022**, *16* (4), 284−290.
(29) Bae, J.; et al. Quantum dot-integrated GaN light-emitting diodes with resolution beyond the retinal limit. *Nat. Commun.* **2022**, *13*, 1862.
(30) Wei, Y.; et al. An overview on enhancing the stability of lead halide perovskite quantum dots and their applications in phosphor-converted LEDs. *Chem. Soc. Rev.* **2019**, *48* (1), 310−350.
(31) Zhang, Q. G.; et al. Ceramic-like stable $CsPbBr^3$ nanocrystals encapsulated in silica derived from molecular sieve templates. *Nat. Commun.* **2020**, *11* (31), 9.
(32) Zhang, Q.; et al. Band Gap Engineering toward Wavelength Tunable $CsPbBr_3$ Nanocrystals for Achieving Rec. 2020 Displays. *Chem. Mater.* **2021**, *33* (10), 3575−3584.
(33) Zhang, Q.; et al. Confined Synthesis of Stable and Uniform $CsPbBr_3$ Nanocrystals with High Quantum Yield up to 90% by High Temperature Solid-State Reaction. *Adv. Opt. Mater.* **2021**, *9*, 2002130.
(34) Zhang, Q.; et al. Suppressing thermal quenching of lead halide perovskite nanocrystals by constructing a wide-bandgap surface layer for achieving thermally stable white light-emitting diodes. *Chem. Sci.* **2022**, *13* (13), 3719−3727.
(35) Lin, Y.; et al. Remarkable Black-Phase Robustness of $CsPbI_3$ Nanocrystals Sealed in Solid SiO_2/AlO_x Sub-Micron Particles. *Small* **2021**, *17*, 2103510.
(36) An, M. N.; et al. Low-Temperature Molten Salts Synthesis: $CsPbBr_3$ Nanocrystals with High Photoluminescence Emission Buried in Mesoporous SiO_2. *ACS Energy Lett.* **2021**, *6* (3), 900−907.
(37) Hou, J.; et al. Liquid-phase sintering of lead halide perovskites and metal-organic framework glasses. *Science* **2021**, *374* (6567), 621−625.
(38) Sun, K.; et al. Three-dimensional direct lithography of stable perovskite nanocrystals in glass. *Science* **2022**, *375* (6578), 307−310.
(39) Wang, B.; et al. Large-Scale Synthesis of Highly Luminescent Perovskite Nanocrystals by Template-Assisted Solid-State Reaction at 800 °C. *Chem. Mater.* **2020**, *32* (1), 308−314.
(40) Lin, J.; et al. Perovskite Quantum Dots Glasses Based Backlit Displays. *ACS Energy Lett.* **2021**, *6* (2), 519−528.
(41) Tsai, H.; et al. Bright and stable light-emitting diodes made with perovskite nanocrystals stabilized in metal-organic frameworks. *Nat. Photonics* **2021**, *15* (11), 843−849.
(42) Wu, S.-H.; et al. Synthesis of mesoporous silica nanoparticles. *Chem. Soc. Rev.* **2013**, *42* (9), 3862.
(43) Liu, X.; et al. Salt melt synthesis of ceramics, semiconductors and carbon nanostructures. *Chem. Soc. Rev.* **2013**, *42* (21), 8237.
(44) Guo, C.; et al. Luminescent properties of $Sr_5(PO_4)_3Cl:Eu^{2+}$, Mn^{2+} as a potential phosphor for UV-LED-based white LEDs. *Appl. Phys. B: Laser Opt.* **2009**, *95* (4), 779−785.
(45) Grivel, J. C. Critical current density improvements in MgB2 superconducting bulk samples by K_2CO_3 additions. *Phys. C: Supercond. Appl.* **2018**, *550*, 1−6.
(46) Bamberger, C. E.; Begun, G. M. The formation of crystalline needles of rutile by flux evaporation. *J. Mater. Sci. Lett.* **1992**, *11* (2), 79−82.
(47) Lin, K.; et al. Dual-Phase Regulation for High-Efficiency Perovskite Light-Emitting Diodes. *Adv. Funct. Mater.* **2022**, *32*, 2200350.
(48) Wang, B.; et al. Postsynthesis Phase Transformation for $CsPbBr_3/Rb_4PbBr_6$ Core/Shell Nanocrystals with Exceptional Photostability. *ACS Appl. Mater. Interfaces* **2018**, *10* (27), 23303−23310.
(49) Park, J.-S.; et al. Alternative Patterning Process for Realization of Large-Area, Full-Color, Active Quantum Dot Display. *Nano Lett.* **2016**, *16* (11), 6946−6953.
(50) Wang, Y.; et al. Direct optical lithography of functional inorganic nanomaterials. *Science* **2017**, *357* (6349), 385−388.

Recommended by ACS

Stable $CsPbBr_3$ Nanocrystals Embedded in SiO_2 for Backlight Display Applications
Xiaoting Liu, Weidong Xiang, *et al.*
APRIL 10, 2023
ACS APPLIED ELECTRONIC MATERIALS
READ

Colloidal $CsPbX_3$ Nanocrystals with Thin Metal Oxide Gel Coatings
Dominic Guggisberg, Dmitry N. Dirin, *et al.*
MARCH 20, 2023
CHEMISTRY OF MATERIALS
READ

Fabrication of High-Performance $CsPbBr_3$ Perovskite Quantum Dots/Polymer Composites via Photopolymerization: Implications for Luminescent Displa...
Xiaotong Peng, Pu Xiao, *et al.*
DECEMBER 19, 2022
ACS APPLIED NANO MATERIALS
READ

Highly Enhanced Photoluminescence Quantum Yield of Phenethylammonium Halide-Passivated Inorganic Perovskite/Cellulose Nanocrystal Films
Yu-Lun Liu, Meng-Lin Tsai, *et al.*
MARCH 14, 2023
ACS SUSTAINABLE CHEMISTRY & ENGINEERING
READ

Get More Suggestions >

https://doi.org/10.1021/acsenergylett.2c02062
ACS Energy Lett. 2023, 8, 151−158